Icing performance of superhydrophobic silicone rubber surfaces by laser texturing

Lie Chen[1], Heng Ping[1], Tao Yang[2], Tao Hu[3], Peter Bennett[1], Zhong Zheng[1], Qibiao Yang[1], Walter Perrie[4], Stuart P. Edwardson[4], Geoff Dearden[4], Dun Liu[1*]

1 Laser Group, School of Mechanical Engineering, Hubei University of Technology, Wuhan, China

2 School of Naval Architecture and Navigation, Wuhan Technical College of Communications, Wuhan, China

3 Hubei Key Laboratory of Green Materials for Light Industry, School of Materials and Chemical Engineering, Hubei University of Technology, Wuhan, China

4 Laser Group, Department of Engineering, University of Liverpool, Brownlow Street, Liverpool L69 3GQ, UK

*Corresponding author. Email: dun.liu@hbut.edu.cn

Abstract: In this paper, the superhydrophobic surfaces of silicone rubber with different microstructure were directly prepared by texturing with a nanosecond fibre laser. The superhydrophobic surfaces have excellent anti-icing performance. Even at 0 ° C, the superhydrophobic surface has a contact angle of ~150° and a rolling-off angle of ~2.5°. The superhydrophobic silicone rubber surfaces with different microstructures have obvious differences in contact behaviours with water droplets at low temperatures. The surface textured with a laser fluence of 10 J cm^{-2} has a larger particle size and more abundant micro-nano particles, which results in a smaller contact area with the water droplet due to greater roughness and root mean square slope. The deeper the small gaps on the superhydrophobic surface, the more time it takes for the change in contact state between the surface and the water droplets. The adhesion strength of the superhydrophobic rubber surfaces with the ice layer were smaller due to the air stored between the surfaces and the ice layer. In particular, the laser textured surface with an laser fluence of 10 J cm^{-2} has the lowest ice adhesion strength due to its layered micro-nano composite structure. After 30 cycles of icing and de-icing, the processed silicone rubber surface still retains excellent hydrophobicity. The superhydrophobic silicone rubber surface has important value in anti-icing and anti-pollution applications.

Keywords: superhydrophobic surface; laser texturing; laser fluence; silicone rubber; icing performance

1. Introduction

Silicone rubber has been widely used in various industries due to its excellent properties, such as temperature resistance, ozone resistance and high electrical resistivity [1, 2]. It has excellent hydrophobicity and can restore its hydrophobicity even after the surface is contaminated [3-5]. Because of these properties, silicone rubber can be widely used in high-voltage power transmission devices [6, 7]. But in fact, as an outdoor insulation product, silicone rubber has also been subjected to severe environmental tests. Especially, the hydrophobic properties of silicone rubber in low-temperature environments are gradually reduced, and it is difficult to prevent moisture and pollutants from adsorbing on the surface [8-10]. Especially in the case of surface icing, the flashover probability of the silicone rubber insulator will increase significantly. Therefore, researchers are more concerned about the wetting properties of silicone rubber at low temperatures in practical use compared to its hydrophobic properties exhibited at room temperature.

Studies have shown that superhydrophobic surfaces have excellent anti-icing properties [11]. Zhan et al. [12] obtained an excellent superhydrophobic surface by CO_2 laser micro-processing on a polytetrafluoroethylene (PTFE) sheet and found that the superhydrophobic surface exhibited excellent dynamic anti-icing performance even at low temperatures. Huang et al. [13] prepared a hydrophobic and anti-icing coating by mixing a silica sol with a fluorine-containing acrylate copolymer on a glass surface. It was found that the icing process on superhydrophobic glass was delayed by 90 minutes at -5.6°C compared to the case of smooth glass. Guo et al. [14] prepared micro, nano and micro-nano combined structures on a ZnO surface. In an ice coating test, it was found that the anti-icing performance of the surface with micro-nano combined structures is better than that of either a micro- or nano-structured surface alone. Jung et al. [15] found that surfaces with nanometre-scale roughness and higher wettability display unexpectedly long freezing delays, at least 1 order of magnitude longer than those of typical superhydrophobic surfaces with larger hierarchical roughness and low wettability. In fact, the existence of the rough structure can

certainly enhance the hydrophobicity to a certain extent, but further investigation is needed regarding the specific influence law of anti-icing performance [16, 17]. Especially when preparing microstructures with superhydrophobic functions, it is also necessary to consider the morphology and size of the micro-structure units [18, 19]. If the morphology and size of the micro-structured units cannot be accurately and effectively controlled, it is difficult to deeply analyse the anti-icing performance of the superhydrophobic surface [20-22]. The current consensus among the researchers is that the superhydrophobic surface with a special rough surface has a significant effect on its anti-icing performance. However, the anti-icing performance of the surface is not only related to the rough surface structure, but also related to the microscopic geometry of the rough structure [23, 24]. Therefore, controlling the microstructure of the superhydrophobic silicone rubber surface and maintaining its good hydrophobic properties at low temperatures is of great significance for the practical application of silicone rubber insulation products.

Laser processing is a simple method for fabricating the superhydrophobic micro-structure on the silicone rubber surface. Emelyanenko et al. [25] obtained a superhydrophobic silicone rubber surface with a contact angle of ~160° (15 μL water droplet) and a rolling-off angle of ~9° (10 μL water droplet) by laser texturing. Then the sample was exposed to UV-ozone treatment, reinforced with fluorooxysilane and dried for 60 min. The contact angle and the rolling-off angle reached ~170° and ~3°. This particular reinforced layer played a very important role in improving the anti-icing performance.

In a previous study as shown in Reference [26], the superhydrophobic silicone rubber surfaces were prepared by a single-step laser processing without any chemical strengthening. The water contact angle and rolling-off angle on the treated silicone rubber surface can reach ~160° and ~3.0° (9 μL water droplet). In addition, it was found that while obtaining the superhydrophobic silicone rubber surface, the microstructure of the surface can also be controlled by laser texturing. It provided the possibility to further study the icephobic properties of superhydrophobic silicone

rubber surface. The icepobic properties of the superhydrophobic silicone rubber surfaces with different surface structures are discussed in this paper. The results provide comprehensive insight into icing phenomena on micro-structured superhydrophobic surfaces, with applications to the development of ice-phobic surfaces.

2. Experimental

2.1 Materials

Silicone rubber (PURESHI GJB-12514) sheets with a thickness of 1 mm were used for all the experiments in this paper. Before laser processing, these samples were cleaned with pure ethanol for 15 minutes in an ultrasonic bath and then dried.

2.2 Experimental equipment

The silicon rubber surface microstructure was fabricated using a nanosecond fibre laser (SPI, 100W EP-Z) with a wavelength of 1064 nm. In the previous study, it was found that the influence of laser pulse width on the wettability of silicone rubber surface is consistent, a pulse width of 200 ns was used in this study. A galvanometer system with an f-theta lens (f=160 mm) scanned the laser beam over the sample surface with a nominal laser focal spot diameter of 50 μm. All experiments were conducted at ambient pressure in air. Consistent with previous experiments, a spot overlap of 70% in the X and Y directions and a repetition rate of 100 kHz was used. The scanning speed can be calculated with the equation,

$$v = (1-\delta) fD = 1500 mm/s$$

where δ is the spot overlap in the X direction (70%), f is the repetition rate (100 kHz), and D is the spot diameter (50 μm).

The refrigeration device shown in Figure 1 was designed to observe the icing process on the superhydrophobic silicone rubber surface. The sample was continuously cooled from room temperature to -18° by using a thermoelectric cooler. The real-time temperature of the water droplets and sample surfaces was measured by an infrared thermometer. The humidity of the test environment was controlled by a humidity controller. A CCD camera was used to record the shape of the water droplets

during the cooling process. In order to avoid the randomness of the freezing delay time and freezing temperature, five samples were prepared for each parameter, and five water droplets were dropped on each sample.

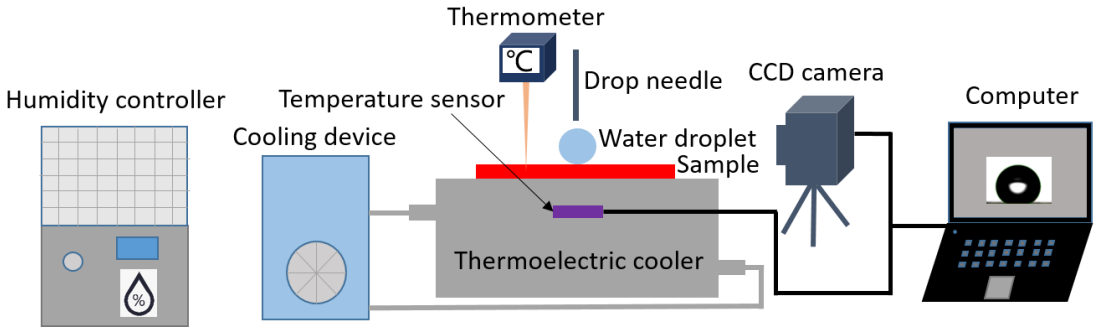

Figure 1. Schematic diagram of the icing monitoring system.

The icing device shown in Figure 2 was designed to measure the ice adhesion strength on the superhydrophobic silicone rubber surface. The device mainly consists of an ice-covered box with a side length of 25 mm and a fixed bracket for holding the sample. A partition with 14 water-permeable holes is fixed in the box. A pull rod with a rally meter is fixed in the center of the partition to measure the tensile adhesion strength of the ice. A tie rod with a rally meter on the side of the box is used to measure the shear adhesion strength of the ice. 10 ml of 2 ° C water was poured into the icing box, and the icing device was placed in a refrigerator at -15 ° C for 1 hour.

The adhesion of ice to the surface of the sample was measured after the water on the sample surface of the sample was frozen, and the ice adhesion strength can be calculated by the equation:

$$\delta = F / s$$

where, F is the force required to remove the ice coating, s is the contact area between the ice coating and the sample surface.

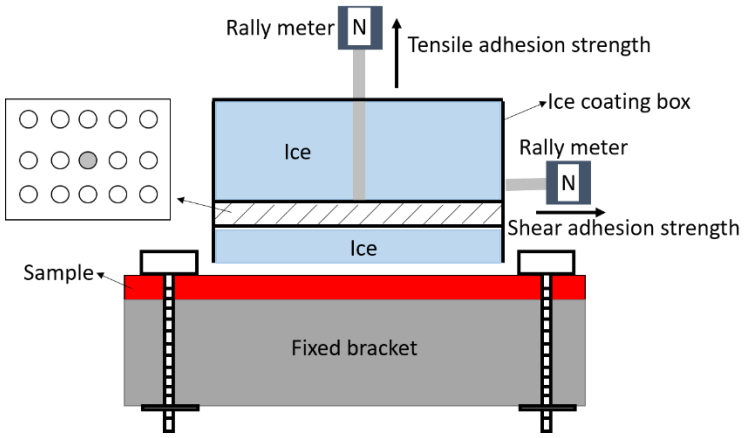

Figure 2. The icing device for measuring the ice adhesion strength on the superhydrophobic silicone rubber surface.

2.3 Surface analysis

The surface wettability was characterized by measuring the contact angle of the sample surface with a camera (NAVITAR 1-6010) and proprietary software (Drop Meter). In view of the excellent hydrophobic properties of the silicone rubber surface after laser irradiation, 9 μL deionized water droplets were used when measuring the surface contact angle at room temperature and low temperature. Five samples were prepared with each laser fluence, and five contact angles and rolling-off angles were measured at different locations on each sample surface. The results were expressed in the form of standard deviation.

To evaluate the morphology of the laser textured surface, a white light interferometric system (BRUKER, Contour GT-K0) and a scanning electron microscopy (SEM) system (HITACHI, SU8010) were employed.

3. Results and Discussion

3.1 Preparation of superhydrophobic silicone rubber surfaces

In our previous studies, a superhydrophobic silicone rubber surface was obtained by using a nanosecond laser, when the laser fluence reached 10 J cm^{-2} or higher [26]. In this paper, the contact behaviour between the superhydrophobic silicone rubber surface with different micro-nano structures and the water droplets at low temperature is discussed.

3.2 Icing property of superhydrophobic silicone rubber surfaces

A 9 μL water droplet at normal temperature was dropped onto the sample surface, which was placed on a thermoelectric cooler. The icing process of water droplets on the superhydrophobic silicone rubber surface at low temperatures was recorded by the camera. The experimental environment temperature was 15°C. The relative ambient humidity was 50%. The timing was started when the sample surface temperature was 13°C. The surface temperature of the sample was measured every 10 seconds using an infrared thermometer during the cooling process.

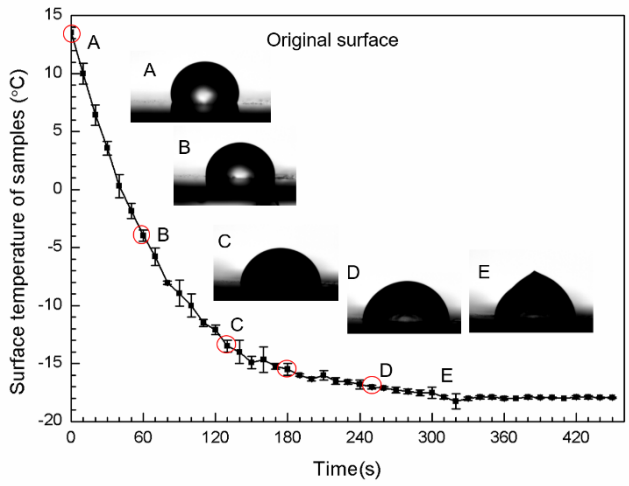

Figure 3. Surface temperature of the original silicone rubber and the morphology of the water droplets during the cooling process.

Figure 3 shows the surface temperature of the original silicone rubber and the morphology of the water droplets during the cooling process. Due to its good thermal insulation properties, the cooling process of silicone rubber presented a nonlinear trend. The surface temperature was lowered to -18°C in 5 minutes and then stabilized. The Insets A, B, C, D and E in Figure 3 exhibit the cooling and icing conditions of the water droplets on the original silicone rubber. Inset A shows the initial state of water droplets on the sample surface. With decreasing temperature, the contact area of the water droplets gradually increased. After cooling for 2 minutes (Inset C), the transparent region in the middle of the water droplet disappeared, which confirmed that the water droplet started to freeze at that time. As shown in Insets D and E, the shape of the water droplet changed significantly during the icing process. The frozen water droplets on the sample surface were more affected by heterogeneous nucleation

[27]. Since the contact state of the water droplet with the untreated sample surface appeared as a Wenzel state, the ice core was formed on the solid-liquid contact surface at the bottom of the water droplet as the surface temperature decreases rapidly, so an ice layer first formed at the bottom. During the continuous cooling process, the icing area gradually extended from the bottom to the top of the water droplet. Finally, after cooling for 4 minutes, the completely frozen water droplets show a distinct conical shape, as shown in Inset E.

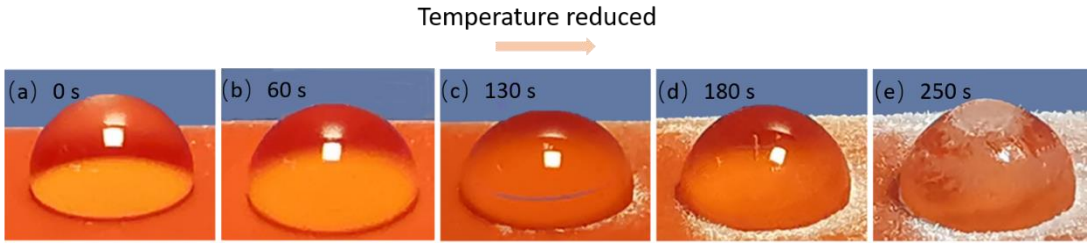

Figure 4. Icing process of the water droplet on the untreated silicone rubber surface

Figure 4 shows that the morphology of the water droplet on the untreated silicone rubber surface during cooling process. With decreasing temperature, the contact area of water droplets gradually increased and the contact angle decreased. Since the heat transfer between the bottom of the water droplet and the sample is the fastest, the ice core was initially formed at the central bottom of the water droplet. Then it gradually filled in the whole contact area and extended upward. Eventually a conical piece of ice with a pointed top was formed.

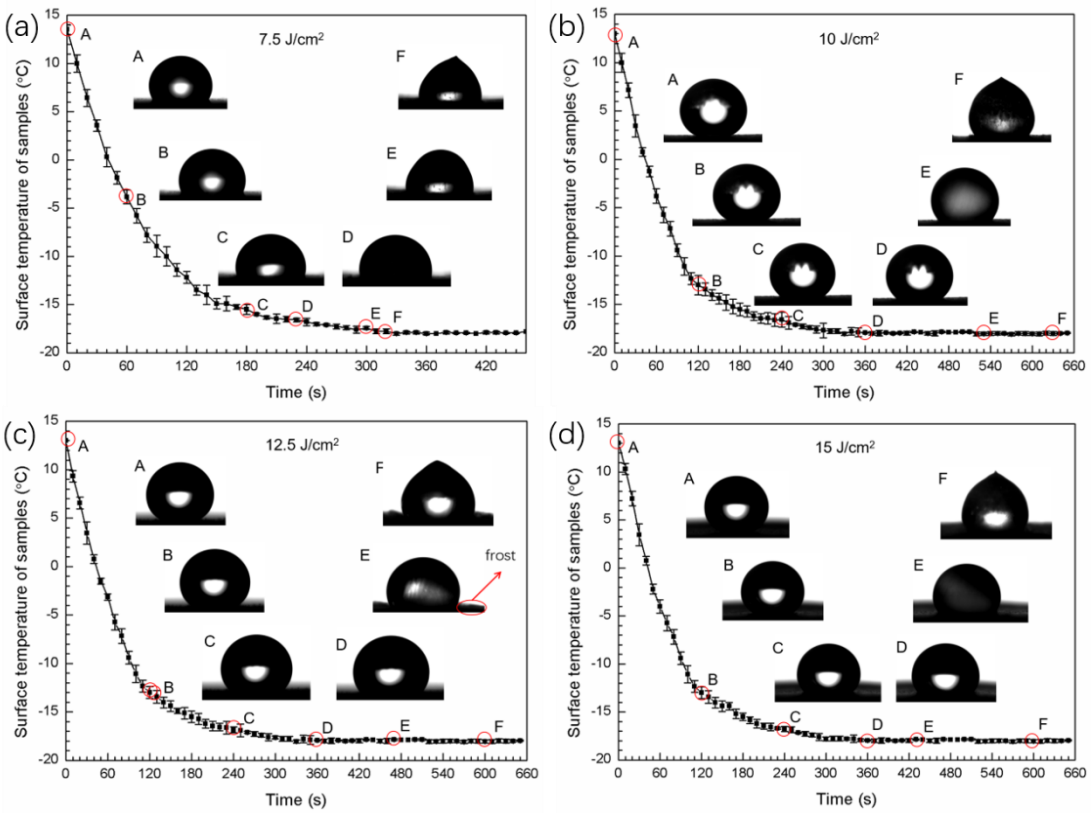

Figure 5. Cooling temperature and water droplet state as a function of the cooling time at laser fluences ranging from 7.5 J cm^{-2} to 15 J cm^{-2}.

Figure 5 shows that the icing process of water droplets on the silicon rubber surfaces irradiated with laser fluences of 7.5 J cm^{-2} to 15 J cm^{-2}. It can be seen that the cooling tendency of the sample surface after laser treatment is substantially consistent with that of the original surface. Although the water temperature would rise sharply at the freezing point when the latent heat was released, the temperature of the sample surface does not show a high scattering during the freezing process [28, 29]. The icing process of water droplets on various surfaces presents a significant difference. On the surface irradiated with a laser fluence of 7.5 J cm^{-2}, the water droplets begin to freeze after 6 minutes of cooling (Inset D in Figure 5 a). This time is extended to 9 minutes when the fluence reaches 10 J cm^{-2} (Inset E in Figure 5 b). However, as the fluence continues to increase, this time is reduced to ~7.5 minutes (Inset E in Figure 5 c). According to the cross-sectional morphology (Figure 10) of the silicone rubber, the roughness and root mean square slope of the surface irradiated with a laser fluence of 10 J cm^{-2} are the largest. A large number of mastoid structures with sharp tops appear

on the surface, which reduces the contact area between the water droplets and the sample surface. When the laser fluence reaches 12.5 J cm^{-2}, the silicone rubber surface is pyrolyzed more completely, which results in decreases of the surface roughness and particle size.

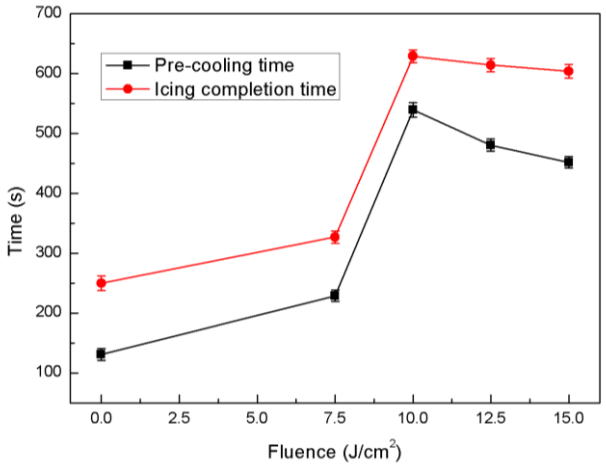

Figure 6. Silicone rubber surface pre-cooling time and complete icing time as processed with different laser fluences.

In previous studies, the time before the ice layer begins to grow has been termed as the pre-cooling time. The transparent area in the middle of the water droplet is due to the transmission of light. The disappearance of the transparent area indicates that the water droplets are beginning to freeze and corresponds to the end of pre-cooling [30]. Figure 6 shows the pre-cooling time and complete icing time of the droplet on the silicone rubber surface processed with different laser fluences. As the fluence increases, the pre-cooling time and the complete icing time of the water droplets increase during the cooling process. The water droplets on the silicone rubber surface irradiated with a laser fluence of 10 J cm^{-2} have the longest pre-cooling and complete icing time, which means that the surface is best for delayed icing. This result indicates that surface wettability is an important factor affecting the performance of delayed icing.

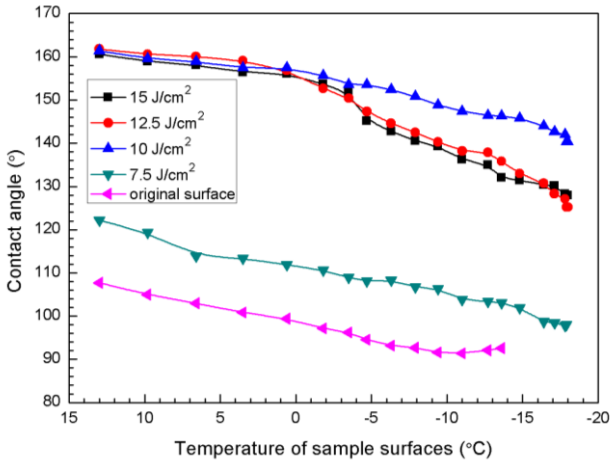

Figure 7. Contact angles of sample surfaces irradiated with different laser fluences during the cooling process.

In view of the change in the contact state of water droplets with the sample surface during the cooling process, the contact angles of the water droplets with the sample before frozen were measured. The results are shown in Figure 7. The results show that the contact angle of each sample surface decreases as the temperature decreases. During the cooling process, the temperature of the rubber surface is lower than the ambient temperature. As shown in Figure 8, the water vapor in the air is liquefied into small water droplets and attaches to the sample surface, which increases the adsorption force on the water droplets. An increase in the contact area of the droplets with the sample surface results in a corresponding decrease in the contact angle [31，32].

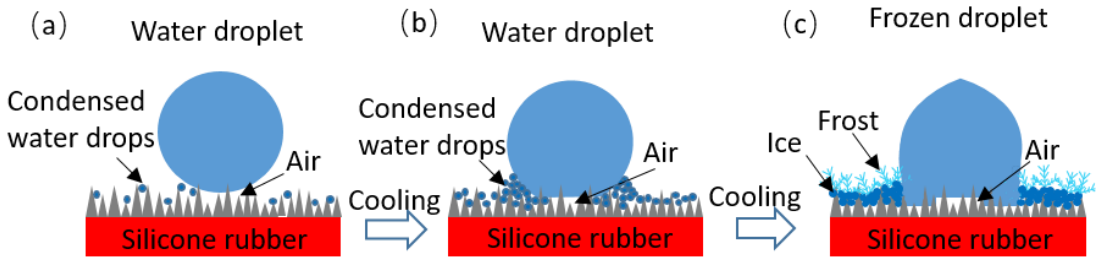

Figure 8. Contact state of the water droplets with the sample surface during the cooling process. (a) Tiny condensation droplets begin to appear on the sample surface; (b) The contact area between the droplet and the sample is increased after the condensation water droplets accumulate to a certain extent; (c) The water droplet on the sample surface is frozen.

Figure 9 shows the morphology of water droplets on the superhydrophobic silicone rubber surface during cooling process. It can be clearly seen that the fine

condensed water droplets formed on the sample surface in the cooling process have a significant pulling effect on the dropped water droplet, which resulting in an increase in the contact area of the water droplet with the sample. It can even be seen that the bubbles are squeezed into the water droplet during this process, as shown in Figure 9 (b). Another noteworthy phenomenon is that the icing process of water droplet on the superhydrophobic silicone rubber surface is not solidified layer by layer from the bottom. As shown in Figure 9 (c), an extremely thin layer of ice is formed on the outer surface of the water droplet, which is solidified from the bottom of the water droplet and gradually extends upwards to wrap the water droplet. It can be considered that the air between the bottom of the water droplet and the sample is not released after the condensed water drops on the sample surface are mixed with the dropped water droplet. Therefore, the contact state of the water droplets with the sample surface exhibits a characteristic state as a "Wenzel state around the bottom and Cassie state at the center", as shown in Figure 8 (b, c). As the ice cores were first formed in the surrounding area at the bottom of the water droplet, the ice layer will extend upward along the surface of the water droplet.

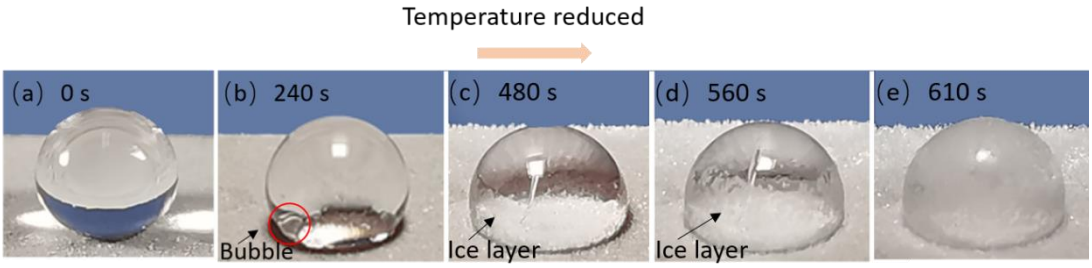

Figure 9. Icing process of the water droplet on the superhydrophobic silicone rubber surface irradiated with a laser fluence of 12.5 J cm^{-2}

In particular, the contact angles of the original surface and the surface irradiated with a laser fluence of 7.5 J cm^{-2} eventually falls below 100°. Since the silicone rubber surface exhibits the typical Wenzel state at this time, the actual contact area of the water droplets with the sample surfaces is large, which results in a decrease in thermal resistance and an increase in heat transfer efficiency. In contrast, although the contact angles of the superhydrophobic silicone rubber surfaces irradiated with laser

fluence of 10-12.5 J cm^{-2} are also lowered during the cooling process, these angles are still greater than 120° before the water droplets frozen. In particular, the silicone rubber surface processed with a laser fluence of 10 J cm^{-2} has the best hydrophobic performance during the cooling process. Before the water droplets frozen, the contact angle of this surface ultimately stabilizes at approximately 140°.

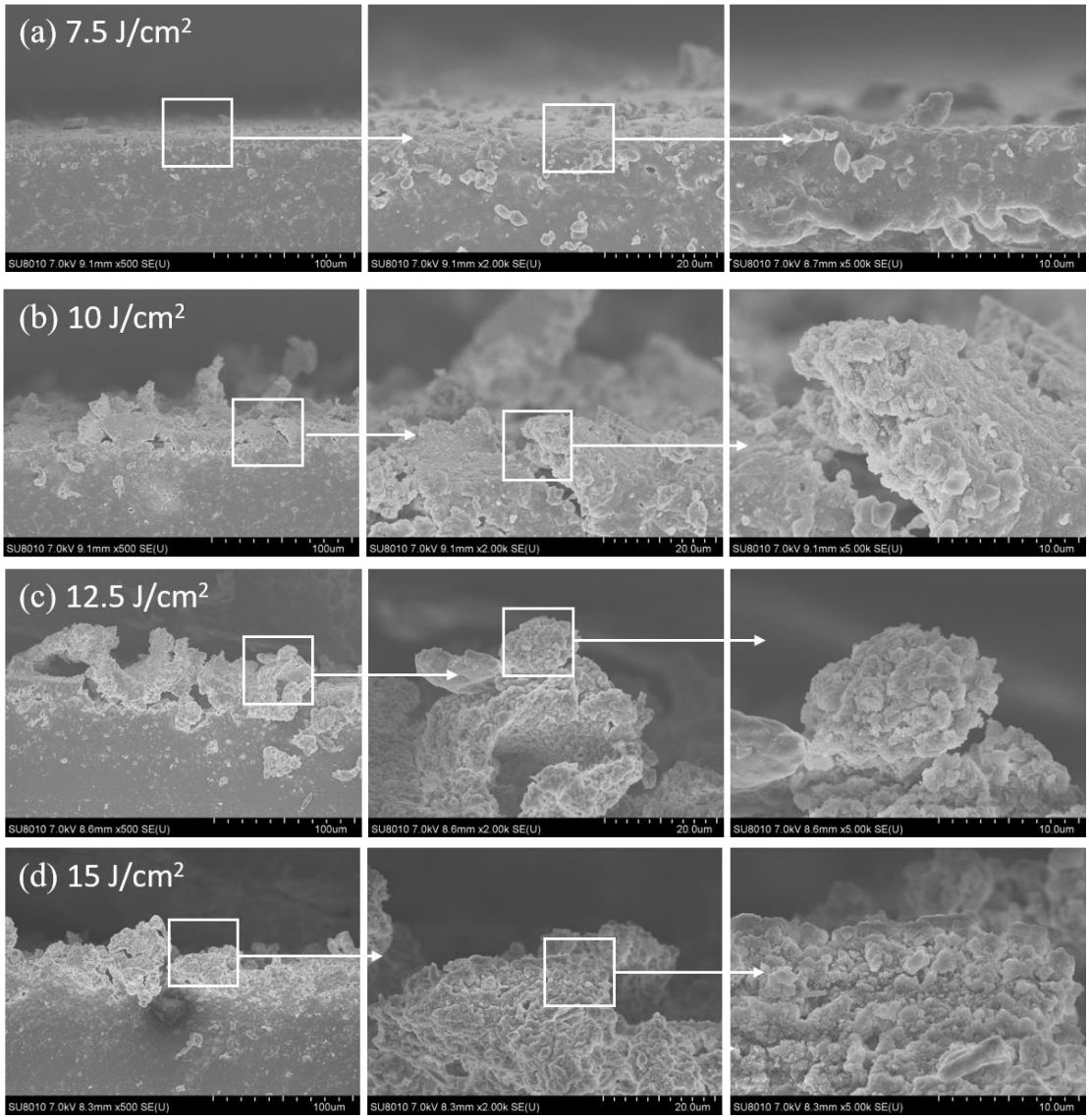

Figure 10. Sectional morphology of samples illuminated with different laser fluences: (a)–(d) laser fluences of 7.5, 10, 12.5, and 15 J cm^{-2}.

Figure 10 shows the sectional morphology of samples illuminated with laser fluences of 7.5, 10, and 12.5 J cm^{-2}. In Figure 10(a–c) on the left, it is clear that as the laser fluence increases, the extent and intensity of the surface cracking of the silicone rubber are increasing. As the fluence increases to 10 J cm^{-2}, sharp peaks on the

microstructures begin to emerge while the nano mastoid structures appear (Figure 10(b)). As the laser fluence increases to 12.5 J cm^{-2}, the size of the mastoids decreases to ~100 nm and then remains stable. However, the peak of the micro-structure on the silicone rubber surface is ablated by the large laser energy. The particles on the sample surface are finer but more rounded. It was found in previous research that both the roughness and root mean square slope show a tendency to rise, decrease and then remain stable as the laser fluence increases. In particular, when the laser fluence is 10 J cm^{-2}, the roughness and root mean square slope reach maximum values (as shown in Figure 7 and Figure 10 of Reference [26]). And the change trend of the microscopic morphology on the cross section of the silicone rubber is also consistent with this result. Although the change in the micro-nano structure does not change the wettability of the silicone rubber at normal temperatures, but it has a significant effect on the contact state of the silicone rubber with water droplets at low temperatures.

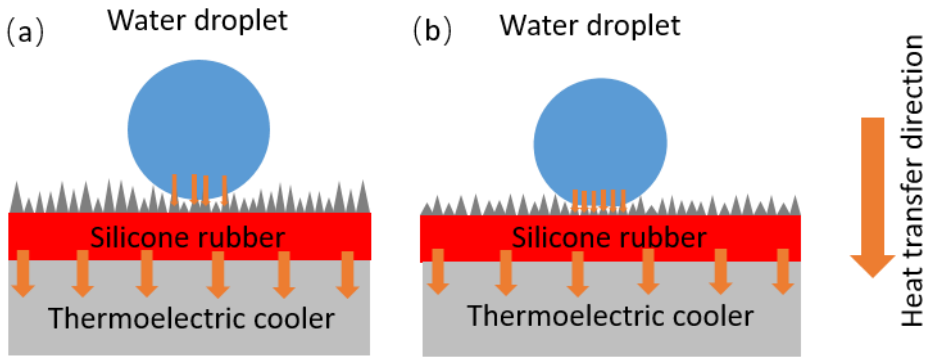

Figure 11. Heat transfer model for water droplets on the sample surfaces with different microstructures. (a) Water droplets on the sample surface with a larger particle size and more abundant micro-nano particles; (b) Water droplets on the surface with smaller and more uniform particles.

Figure 11 shows a heat transfer model for water droplets on the sample surfaces with different microstructures. The laser textured surface with a fluence of 10 J cm^{-2} has a larger particle size and more abundant micro-nano particles compared to the surface with fluences of 12.5-15 J cm^{-2}, which results in a smaller contact area with the water droplet due to greater roughness and root mean square slope. Thus, more air can be trapped, which further reduces the heat transfer efficiency when the surface droplets freeze. Therefore, the surface with a laser fluence of 10 J cm^{-2} offers the longest time of icing delay.

It has been previously observed that when the dropped water droplet is cooled together with the sample, the contact state of the water droplet with the sample is affected by the continuous condensation of fine water droplets. In order to further evaluate the contact state of the water droplets with the surface of the low temperature sample, and to eliminate the interference of the continuously condensed water droplets as much as possible, the contact angle and rolling-off angle on the silicone rubber surface at low temperatures were measured. Before this measurement, the temperature of the sample was lowered to a certain temperature and maintained by adjusting the power of the refrigerator. The visible water droplets condensed on the surface of the sample were blown away by an air blower. The results of the contact angle and the rolling-off angle measured by applying 9 μL of water droplet at a temperature of 2℃ are shown in Figure 12.

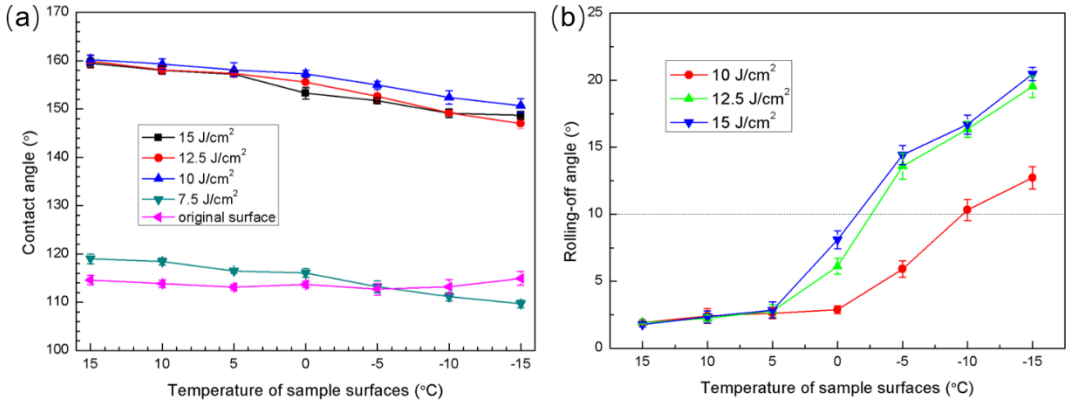

Figure 12. (a) Contact angle and (b) rolling-off angle of sample surfaces at different temperatures (applying a 9 μL water droplet at a temperature of 2 ℃)

The experimental results show that the contact angle of the surface decreases as the temperature decreases. In fact, although the visible large condensed water droplets on the sample surface were removed by the blower, the tiny water droplets condensed in the small gaps of the sample surface cannot be completely removed. Moreover, the lower the temperature of the sample, the more fine water droplets will be accumulated. This problem cannot be completely avoided in the actual natural environment. Because as long as there is a temperature difference between the sample and the environment, the water vapour in the air will be condensed on the sample surface. As shown in Figure 13, the contact of the dropped water droplet with the condensed

water droplets causes an increase in the contact area between the water droplet and the sample surface, which results in a decrease in the contact angle at low temperatures.

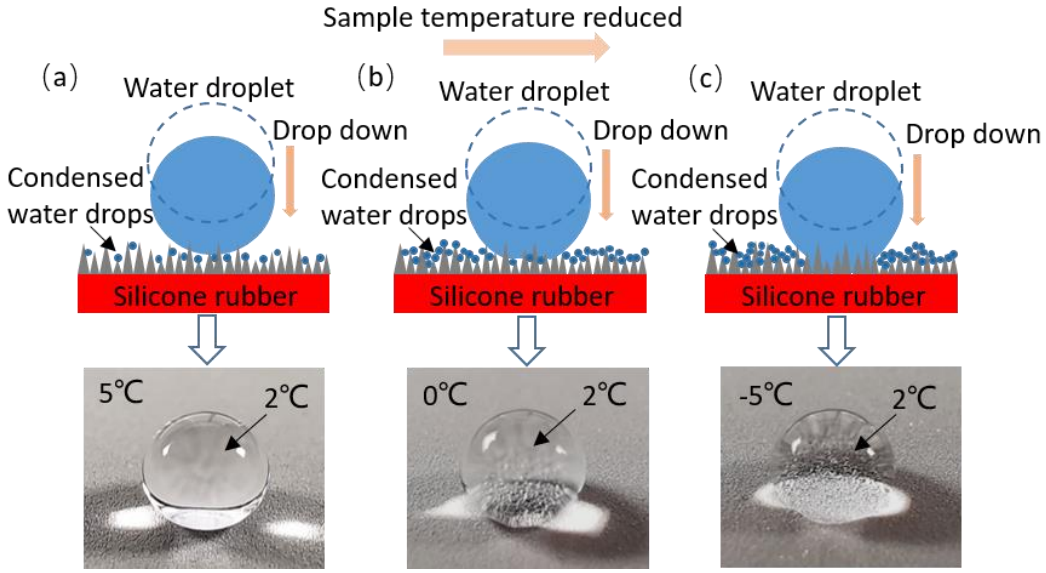

Figure 13. The state of tiny condensed water droplets in the grooves of different surfaces. (a): A small amount of condensation water droplets attach to the small gaps on the sample surface, and the contact state between the water droplet and the sample surface still shows the Cassie state; (b) and (c): As the temperature of the sample surface further decreases, the tiny condensed water accumulated in the fine gaps mixes with the dripping water droplets, and the contact state between the water droplet and the sample surface is changed to the Wenzel state.

The results also show that the infiltrated states of the superhydrophobic silicone rubber surfaces processed with laser fluence of 10-15 J cm^{-2} are still significantly better than that of the original surface at the low temperature. In particular, for the sample surface treated with a laser fluence of 10 J cm^{-2}, the surface contact angle is still greater than 150° when the temperature of the sample surface is lowered to -15°C. This result is consistent with the previous results shown in Figure 7.

Another phenomenon worthy of attention is that the rolling-off angles of each sample surface processed with laser fluence of 10-15 J cm^{-2} are very similar before the temperature is lowered to 5°C (Figure 12(b)). However, following the temperature drop to 0°C, the changes in the rolling-off angle on each sample surface are obviously different. The rolling-off angle of the surface processed with laser fluence of 12.5-15 J cm^{-2} rises significantly faster. When the sample temperature drops to -5°C, the rolling-off angle of these surfaces has reached 10°. In contrast, the rolling-off angle on

the silicone rubber surface irradiated with a laser fluence of 10 J cm^{-2} rises more slowly. The rolling-off angle of the sample is approximately 10° when the temperature drops to -10°C and rises to approximately 12° when the temperature is further reduced to -15°C.

In the initial stage of cooling, there is only a small amount of tiny condensed water droplets in the small gaps on the superhydrophobic sample surface. The presence of these tiny droplets causes a small decrease in the contact angle and a small increase in the rolling-off angle of the sample surface. Nevertheless, the contact of the water droplets with the surface still exhibits the Cassie state. Under normal circumstances, when the temperature of the superhydrophobic surface is the same as the ambient temperature and the micro gaps on the surface remain dry, the capillary force will expel the water meniscus from the pores. However, when the sample temperature is much lower than the air temperature, the liquefied water vapor in the air adheres to the texture of the sample surface, which resulting in the micro gaps on the sample surface to be wetted. At this time, the dripping water droplet would penetrate into the fine gaps under the influence of capillary action [33, 34]. The contact of the water droplets with the sample changes to the Wenzel state, and the rolling-off angle increases rapidly. Observing the rolling-off angle of each surface as shown in Figure 12 (b), it can be found that for the sample surface irradiated with laser energy of 10-15 J cm^{-2}, the rolling-off angle on the surface irradiated with a laser fluence of 15 J cm^{-2} increases the fastest. Although the wettability of the surface of these samples is very similar at normal temperatures, the microscopic state of each surface is quite different. Because of the small particle size of the sample surface, the tiny water droplets accumulated in the gaps of the surface irradiated with a laser fluence of 15 J cm^{-2} reach the critical state more quickly, resulting in a faster transition of the contact state with the water droplets to the Wenzel state. In contrast, due to its greater roughness and root mean square slope, the small gaps on the sample surface irradiated with a laser fluence of 10 J cm^{-2} are deeper. It takes more time to change the contact state between the sample surface and the water droplet. Finally, the anti-icing performance is reduced when the temperature is extremely low and the

superhydrophobic surface is completely wetted by the condensated film.

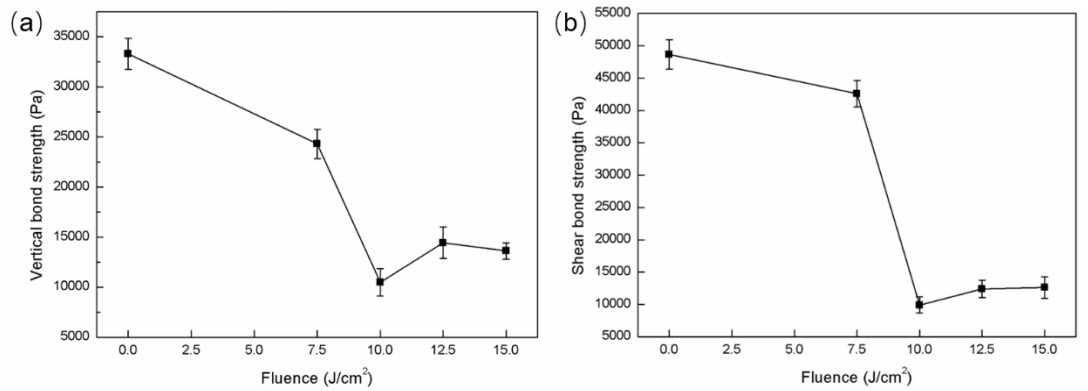

Figure 14. Ice adhesion strength on the silicone rubber surfaces processed with different laser fluences.

In view of the difference in contact state of water droplets on the silicone rubber surface processed with different laser fluences, the ice tensile adhesion strength and shear adhesion strength of the sample surfaces were measured. As shown in Figure 14, the ice adhesion strength of the original surface is much larger than that of the laser-processed silicone rubber surfaces with the same ice layer area and thickness. In particular, the ice adhesion strength of the silicone rubber surface irradiated with laser fluence of 10 J cm^{-2} is the lowest. This result is also consistent with the results of the previously observed contact angles. In the previous model, we thought that the gaps on the superhydrophobic surfaces actually act as gas reservoirs. In the case where the overall ice layer volumes are the same, the actual contact areas of the superhydrophobic surfaces with the ice layer are smaller, thereby resulting in smaller ice layer adhesion strength. Since the gaps on the surface microstructures of the sample treated with a fluence of 10 J cm^{-2} is the deepest, the actual contact area between the ice and the sample surface is the smallest, and the ice adhesion strength is also the smallest. This also proves the previous analysis of the contact states of water droplets with each sample surface.

The mechanical resistances of the silicone rubber surfaces textured with different laser fluences were measured according to the method mentioned in Reference [25]. As shown in Figure 15, the processed samples were placed in a container filled with deionized water and then placed in a refrigeration unit. The deionized water was frozen in an environment at a temperature of -20 °C for 30 minutes, and an ice layer

with a thickness of 7 mm was obtained. The container was then taken out and thawed for 30 minutes in an environment of T = 20 °C. After repeating the desired icing/de-icing cycles, the sample was taken from the container and dried with an ashfree filter paper. After every five cycles, the contact angles and rolling-off angles of the sample surfaces were measured in the laboratory air (temperature 20 °C, relative humidity 50%) , and the results are shown in Figure 16.

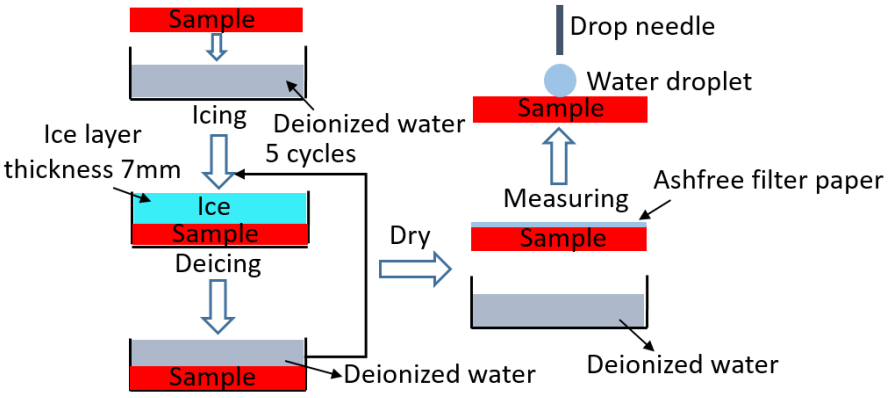

Figure 15. Icing/de-icing process on the silicone rubber surfaces textured with different laser fluences

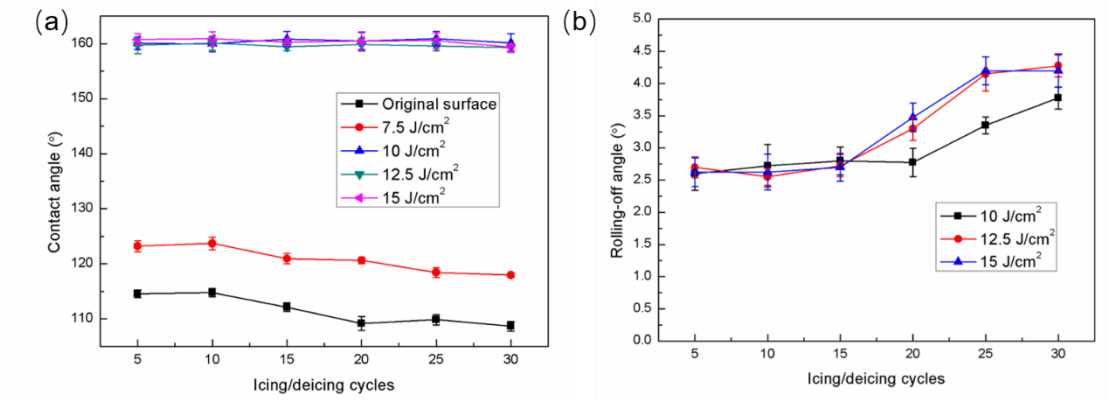

Figure 16. (a) Contact angles and (b) rolling-off angles of the sample surfaces after icing/de-icing cycles

The results show that as the icing/de-icing cycle increases, the contact angles of the original surface and the surface irradiated with a laser fluence of 7.5 J cm^{-2} significantly decrease, while the contact angles of the superhydrophobic surfaces (irradiated with laser fluences of 10-15 J cm^{-2}) remain substantially stable, and the rolling-off angles increase only slightly. In particular, after 30 times of icing/de-icing, the contact angle of the silicone rubber surface irradiated with a laser fluence of 10 J cm^{-2} was maintained at ~160°, and the rolling-off angle was ~ 3.5°. It indicates that the surface microstructure of the prepared superhydrophobic silicone rubber has an

excellent mechanical resistance and durability for anti-icing.

4. Conclusions

It was shown that superhydrophobic surfaces can be generated on silicone rubber in air using a low-cost pulsed nanosecond fibre laser. The wettability of the processed silicone rubber surfaces developed from hydrophobic to superhydrophobic when the laser fluence reached 10 J cm^{-2} or higher. However, the microstructure of the superhydrophobic silicone rubber surfaces by laser texturing with different laser fluences shows significant differences. The superhydrophobic surface has better anti-icing performance, including a longer time for delay icing and better hydrophobic performance at low temperatures. Since the water droplets on the superhydrophobic surface were affected by the tiny condensed water droplets on the sample surface during the cooling process, the contact state of water droplets with the sample surface has changed, which shows a state as a "Wenzel state around the bottom and Cassie state at the centre". And this state is maintained until the water droplets completely solidify into ice.

In addition, the microstructure has an important influence on the icing process of water droplet on the superhydrophobic surfaces. The superhydrophobic silicone rubber surface processed by a laser fluence of 10 J cm^{-2} takes the longest time to freeze, which can reach more than 7 minutes. Although the contact angle of the sample surface is slightly reduced due to the influence of the condensed water, the contact angle of this sample surface can be kept at approximately 140° when the temperature is lowered to -18°C. The laser textured surface with a fluence of 10 J cm^{-2} has a larger particle size and more abundant micro-nano particles than the surface with fluences of 12.5-15 J cm^{-2}, which results in a smaller area contact with the water droplets due to its greater roughness and root mean square slope.

When measuring the contact angle and rolling-off angle of each surface at different temperatures, it is found that the contact angle decreases with decreasing temperature, and the rolling-off angle increases. As the temperature decreases, the dropped water droplets will completely penetrate into the fine gaps under the influence of capillary action when the condensed tiny water droplets accumulated in

the surface gaps reach a critical value. The contact state of the water droplets with the sample surface changes from the Cassie to the Wenzel state, so the rolling-off angle increases rapidly. Due to the larger roughness and root mean square slope, the sample surface textured with a laser fluence of 10 J cm^{-2} has deeper gaps and sharper peaks, which results in a longer time for transition of the contact state with water droplet. The anti-icing performance would be reduced when the temperature is extremely low and the superhydrophobic surface is completely wetted by the condensated water film. The adhesion strength of the superhydrophobic rubber surfaces with the ice layer were smaller due to the air stored between the surfaces and the ice layer. In particular, the laser textured surface with an laser fluence of 10 J cm^{-2} has the lowest ice adhesion strength due to its layered micro-nano composite structure. The processed silicone rubber surface still maintains excellent superhydrophobic property after 30 cycles of icing/de-icing. And the surface irradiated with a laser fluence of 10 J cm^{-2} has a better mechanical resistance. In addition, the low scattering of the contact angles and rolling-off angles of the superhydrophobic sample surfaces demonstrates a uniform surface wettability.

It has been presented that the surfaces with micro-nano combined structures and suitable particle sizes have better anti-icing performance. These results provide comprehensive insight into icing phenomena on micro-structured superhydrophobic surfaces, with applications for the development of ice-phobic surfaces.

Acknowledgements:

This work was supported by the National Natural Science Foundation of China (Grant Nos. 51703053, 51775176). The authors are grateful to Mr John Riches for helping with the analysis of the surface properties of silicone rubber.

References

[1] Xie Z H, Zeng F W and Xiao J B 2011 Progress and Research Progress of Silicone Rubber *Special Purpose Rubber Products* **32** 69-72.

[2] Wang L, Gong Q, Zhan S, Jiang L and Zheng Y 2016 Robust Anti-Icing Performance of a Flexible Superhydrophobic Surface *Adv. Mater.* **28** 7729-7735.

[3] Momen G and Farzaneh M 2011 Survey of micro/nano filler use to improve

silicone rubber for outdoor insulators *Rev. Adv. Mater. Sci.* **27** 1-13.

[4] Siderakis K, Agoris D and Gubanski S 2008 Salt Fog Evaluation of RTV SIR Coatings With Different Fillers *IEEE T. Power Delivery* **23** 2270-2277.

[5] Guan Z, Niu K, Wang L, Mei H and Wei X 2012 Influence of ambient humidity on hydrophobicity transfer of silicone rubber material *High Volt. Eng.* **38** 2030-2036.

[6] Zhang F Z, Peng G M, Wang L M and Guan Z C 2010 Influence of Environmental Temperature on Flashover Voltage of Composite Insulator *High Volt. Eng.* **36** 1119-1123.

[7] Guan Z C, Peng G M, Wang L M, Jia Z D and Zhang R B 2011 Application and key technical study of composite insulators *High Volt. Eng.* **37** 513-519.

[8] Liu Z H 2006 Current Status of Composite Insulators and Its Application Prospect in UHV Transmission Lines *Power System Tech.* **30** 1-7.

[9] Wei Y H, Wu L H and Wang C H 2006 Analysis of the influence of atmospheric environment on the hydrophobicity of synthetic insulators *High Volt. Tech.* **32** 31-34.

[10] Guo H 2006 Application and Operation of Composite Insulators in China *Electric Power Equipment* **7** 43-45.

[11] Lv J, Song Y, Jiang L and Wang J 2014 Bio-Inspired Strategies for Anti-Icing *ACS Nano* **8** 3152-3169.

[12] Zhan Y L, Ruan M, Li W, Li H, Hu L Y, Ma F M, Yu Z L and Feng W 2017 Fabrication of anisotropic PTFE superhydrophobic surfaces using laser microprocessing and their self-cleaning and anti-icing behavior *Colloids Surf. A.* **535** 8-15.

[13] Huang Y F, Hu M J, Yi S P, Liu X H, Li H B, Huang C, Luo Y B and Li Y 2012 Preparation and characterization of silica/fluorinated acrylate copolymers hybrid films and the investigation of their icephobicity *Thin Solid Films* **520** 5644-5651.

[14] Guo P, Zheng Y M, Wen M X and Song C 2012 Icephobic/ Anti-Icing Properties of Micro/ Nanostructured Surfaces *Adv. Mater.* **24** 2642-2648.

[15] Jung S, Dorrestijn M, Raps D, Das A, Megaridis C M and Poulikakos D 2011 Are superhydrophobic surfaces best for icephobicity *Langmuir* **27** 3059-3066.

[16] Farhadi S, Farzaneh M and Kulinichm S A 2011 Anti-icing performance of superhydrophobic surfaces *Appl. Surf. Sci.* **257** 6264-6269.

[17] Zou M, Beckford S, Wei R, Ellis C, Hatton G and Miller M A 2011 Effects of surface roughness and fluence on ice adhesion strength *Appl. Surf. Sci.* **257** 3786-3792.

[18] Wang J, Yang H, Wang L P and Dong P 2017 Design of anti-icing hydrophobic microstructure surface *Acta Aeronautica Et Astronautica Sinica* **38** 40-47.

[19] Basu B J and Manasa J 2011 Effect of deposition parameters on the wettability and microstructure of superhydrophobic films with hierarchical micro–nano structures *J. Colloid. Interf. Sci.* **363** 655-662.

[20] He M, Wang J, Li H and Song Y 2011 Super-hydrophobic surfaces to condensed micro-droplets at temperatures below the freezing point retard ice/frost formation, *Soft Matter* **7** 3993-4000.

[21] Jindasuwan S, Nimittrakoolchai O, Sujaridworakun P, Jinawath S and Supothina S 2009 Surface characteristics of water-repellent polyelectrolyte multilayer films containing various silica contents *Thin Solid Films* **517** 5001-5005.

[22] Kulinich S A, Farhadi S, Nose K and Du X W 2011 Superhydrophobic surfaces: are they really ice-repellent *Langmuir* **27** 25-29.

[23] Bengaluru S S, Kondrashov V, Rühe J and Varanasi K K 2016 Low Ice Adhesion on Nano-Textured Superhydrophobic Surfaces under Supersaturated Conditions *ACS Appl. Mater. Inter.* **8** 12583-12587.

[24] Cao L, Jones A K, Sikka V K, Wu J and Gao D 2009 Anti-icing superhydrophobic coatings *Langmuir* **25** 12444-12448.

[25] Emelyanenko A M, Boinovich L B, Bezdomnikov A A, Chulkova E V and Emelyanenko K A 2017 Reinforced superhydrophobic coating on silicone rubber for longstanding anti-icing performance in severe conditions *ACS Appl. Mater. Interfaces* **9** 24210-24219.

[26] Chen L, Wang X, Yang T, Ping H, Peter B, Zheng Z, Yang Q B, Walter P, Stuart P. E, Geoff D and Liu D 2018 Superhydrophobic micro-nano structures on silicone rubber by nanosecond laser processing *J. Phys. D. Appl. Phys.* **51** 445301.

[27] Nitsch K 2009 Thermal analysis study on water freezing and supercooling *J. Therm. Anal. Calorim.* **95** 11-14.

[28] Alizadeh A, Yamada M, et al 2012 Dynamics of Ice Nucleation on Water Repellent Surfaces *Langmuir* **28** 3180-3186.

[29] Yin L, Xia Q, et al 2010 In situ investigation of ice formation on surfaces with

representative wettability *Appl. Surf. Sci.* **256** 6764-6769.

[30] Shen Y, Tao H, Chen S, Zhu L, Wang T and Tao J 2014 Icephobic/anti-icing potential of superhydrophobic Ti6Al4V surfaces with hierarchical textures *RSC Adv.* **5** 1666-1672.

[31] Van D T, Andrew D, Thomas J W, Ji L, Robert W K, Jonathan S, Patrick J S, Emre E, Colm C and Jonathan D S 2016 Laser textured superhydrophobic surfaces and their applications for homogeneous spot deposition *Appl. Surf. Sci.* **365** 153-159.

[32] Alizadeh A, Yamada M, Li R, Shang W, Otta S, Zhong S, Ge L H, Dhinojwala A, Conway K R, Bahadur V, et al 2012 Dynamics of Ice Nucleation on Water Repellent Surfaces *Langmuir* **28** 3180-6.

[33] Metya A K and Singh J K 2018 Ice adhesion mechanism on lubricant-impregnated surfaces using molecular dynamics simulations *Mol. Simulat.* **45** 394-402.

[34] Howard A S 2012 Ice-Phobic Surfaces That Are Wet *ACS Nano* **6** 6536–6540.